DNA sliding and loop formation by *E. coli* SMC complex: MukBEF

Man Zhou

Department of Biochemistry, University of Oxford, Oxford, OX1 3QU, UK

ABSTRACT

SMC (structural maintenance of chromosomes) complexes share conserved architectures and function in chromosome maintenance via an unknown mechanism. Here we have used single-molecule techniques to study MukBEF, the SMC complex in *Escherichia coli*. Real-time movies show MukB alone can compact DNA and ATP inhibits DNA compaction by MukB. We observed that DNA unidirectionally slides through MukB, potentially by a ratchet mechanism, and the sliding speed depends on the elastic energy stored in the DNA. MukE, MukF and ATP binding stabilize MukB and DNA interaction, and ATP hydrolysis regulates the loading/unloading of MukBEF from DNA. Our data suggests a new model for how MukBEF organizes the bacterial chromosome *in vivo*; and this model will be relevant for other SMC proteins.

1. Introduction

The SMC (structural maintenance of chromosome) complexes share conserved architectures and function in chromosome maintenance throughout all kingdoms of life, including heterodimeric condensin, cohesin, and SMC5/6 in eukaryotes and homodimeric SMC complex in prokaryotes, such as MukBEF in *E. coli* [1–3]. SMC dimers adopt a large ring structure containing a ~50-nm antiparallel coiled-coil "arm" with a hinge dimerization domain and an ABC-type ATPase head domain [4]. The distinctive and conserved molecular architecture suggests a common principle of SMC complex function. One mechanism explaining the formation of DNA loops is provided by the loop extrusion model, which proposes SMC proteins to act as loop-generating motors during iterative cycles of ATP hydrolysis. Single molecule assays have demonstrated that SMC protein translocates along DNA in an ATP-dependent manner [5–7]; in contrast, other studies have reported that SMC protein slides along DNA in an ATP-independent manner [8,9]. Meanwhile, there are reports of real-time visualization of symmetric/asymmetric DNA loop extrusion by condensin and symmetric loop extrusion by cohesin, albeit under small external force [10–13].

However, the physical nature of DNA as a highly dynamic polymer with properties that may profoundly affect the function of SMC proteins. Overlap of two DNA polymers in cylindrical confinement significantly reduces their conformational entropy, and theoretical simulations suggest that entropic forces can drive chromosome segregation under the right physical condition [14–19]. Moreover, experimental studies have already well characterized the *E. coli* nucleoid dynamics in living cells [20,21]. Different simulation-based models have been proposed: one

Brownian dynamics simulation suggested that chromatin loops can be efficiently formed by non-equilibrium dynamics of DNA on the diffusive sliding of molecular slip links [22]. In contrast, other simulation-based models predict DNA loops can be actively extruded by ATP powered SMC motor proteins [23–27].

Here, we generated fluorescently labelled MukB (Fig.1A) and exploited two complementary single-molecule assays with total internal reflection fluorescence (TIRF) microscopy to probe the function of the *E. coli* SMC complex, MukBEF, by either immobilizing DNA or MukB on the surface (Fig.1B).

2. Materials and methods

2.1. Fabrication of flow cell

The glass slides and coverslips were super-cleaned with acetone, 1 M NaCl and MiliQ water solutions. The bottom coverslip was functionalized with an amino-group in the 2% 3-aminopropyltheithoxysilane (440140, Sigma) in acetone for 10 min. Then surfaces were PEGylated by applying a viscous mixture of PEG and biotin-PEG to one side of the coverslip at room temperature for 3 h and washed intensively with MiliQ water.

Four 1.5 mm holes were drilled in the glass slide in the pattern show in Fig. 1B, and 1.5 mm diameter tubing was glued into each hole with epoxy resin glue. Afterwards, double-side tape was stack between coverslip and drilled glass slide to make a flow cell.

2.2. Double-tethered λDNA for single-molecule study

The double biotin-labelled λDNA preparation was similar as ref. [10]. Flow cells were first incubated with 0.3 mg/ml neutravidin in T50 buffer (20 mM Tris-HCl, pH = 7.5, 50 mM NaCl) for 1 min and washed with 400 μl T50 buffer. 50 μl of 20 pM double biotin-labelled λDNA (ThermoFisher Scientific; SD0011) was introduced into flow cells at 1–2 μl/min in T50 buffer with 200 nM Sytox orange (ThermoFisher Scientific; S11368). Excess DNA was washed off with T50 buffer once optimum DNA density was achieved.

10–100 nM MukB-Cy5 in the crude image buffer without PCA/PCD and Trolox (20 mM Tris-HCl, pH = 7.5, 50 mM NaCl, 0.3mg/BSA, 2 mM DTT, 400 nM Sytox orange) was introduced at 1 μl/min, to observe DNA compaction. 10 nM MukF, 20 nM MukE and 1 mM ATP-Mg^{2+} in the imaging buffer (20 mM Tris-HCl, pH = 7.5, 50 mM NaCl, 0.3 mg/BSA, 2 mM DTT, 2.5 mM PCA, 50 nM PCD, 1 mM Trolox and 400 nM Sytox orange) was introduced in the perpendicular direction.

For EQ mutation, 10 nM MukB^{EQ}-Cy5, 10 nM MukF, 20 nM MukE and 1 mM ATP-Mg^{2+} in the imaging buffer (20 mM Tris-HCl, pH = 7.5, 50 mM NaCl, 0.3 mg/BSA, 2 mM DTT, 2.5 mM PCA, 50 nM PCD, 1 mM Trolox and 400 nM Sytox orange) was introduced into the flow cell, and then 10 nM MukF, 20 nM MukE and 1 mM ATP-Mg^{2+} in the imaging buffer (20 mM Tris-HCl, pH = 7.5, 50 mM NaCl, 0.3 mg/BSA, 2 mM DTT, 2.5 mM PCA, 50 nM PCD, 1 mM Trolox and 400 nM Sytox orange) was introduced in the perpendicular direction.

For DA mutation, 100 nM MukB^{DA} was introduced in the flow cell.

2.3. Immobilization of His$_6$-tagged MukB for single-molecule study

Flow cell was firstly incubated with 0.3 mg/ml neutravidin in T50 buffer (20 mM Tris-HCl, pH = 7.5, 50 mM NaCl) for 1 min and washed with 400 μl T50 buffer. Afterwards, 2 μg/ml Biotinylated Anti-His Antibody (Penta-His Biotin Conjugate; Qiagen; No. 34440) in T50 buffer was introduced into flow cells at 50 μl/min, then wash immediately with 300ul T50 buffer. 5 nM - 10 nM MukB was incubated with 100 pM λDNA or 100 pM 44 kb plasmid (p412-insert95 mats, a gift from Jaco van der Torre in Cees Dekker group) in T50 buffer for 20 min at room temperature (22°C), then introduced into the flow cell at 5–10 μl/min to immobilize His$_6$-tagged MukB on the surface.

2.4. Single-molecule Imaging

Single-molecule TIRF experiments were performed on a custom-built, objective-type TIRF microscope. A green laser (532-nm Cobolt Samba; Cobalt) and a red laser (635-nm CUBE; Coherent) were combined using a dichroic mirror and coupled into a fibre optic cable. The

output of the fibre was focused into the back focal plane of the objective (magnification of 100×, oil immersion, N.A. = 1.4, f/26.5; UPlanSApo, Olympus) and displaced perpendicular to the optical axis such that laser light was incident at the slide/solution interface at greater than the critical angle, creating an evanescent excitation field. Illumination powers were set as low as possible to avoid the photo damage of DNA.

Fluorescence emission was collected by the objective and separated from the excitation light by a dichroic mirror (545 nm/650 nm; Semrock) and clean-up filters (545-nm long pass, Chroma; 633/25-nm notch filter, Semrock). The emission signal was focused on a rectangular slit to crop the image and then spectrally separated, using a dichroic mirror (630-nm long pass; Omega), into two emission channels that were focused side-by-side onto an electron multiplying charge coupled device (EMCCD) camera (iXon 897; Andor). The EMCCD was set to an EM gain of 300, corresponding to an approximate real gain of four counts per photon. Each pixel on the EMCCD corresponded to a 96 × 96 nm region in the imaging plane.

2.5. Image analysis and data processing

Fluorescence images were analysed by ImageJ software. The background of image was firstly subtracted, and a binary mask was generated by applying thresholding to select fluorescent molecules. Afterwards, identified ranges were generated by applying 'analyse particles' on the mask, that were between 9 and 300 pixels and with the circularity between 0.2 and 1. The intensity of selected ranges was calculated for number determination of MukB and MukB^{EQ}.

2.6. Expression and purification of the MukBEF His$_6$-tagged proteins

Wild-type MukB was His$_6$-tagged at the C-terminus and was expressed from plasmid pET-21(+) (Novagen #69740) in C3013I cells (NEB). For Immobilized His$_6$-tagged MukB, a flexible 10(glycine-serine) linker was introduced between His tag and MukB. 2L cultures were grown in LB with 100 μg/ml carbenicillin at 37 °C to OD600–0.6 and induced by adding IPTG at final concentration of 0.4 mM. After 4 h at 30 °C, cells were harvested by centrifugation, suspended in 30 ml lysis buffer (50 mM HEPES pH 7.5, 300 mM NaCl, 5% glycerol, 10 mM imidazole) supplemented with 1 tablet Complete mini-protease inhibitor cocktail (Roche) and sonicated. Cell debris was removed by centrifugation and target proteins were first purified by TALON Superflow resin. Then, the fractions from TALON were diluted to 100 mM NaCl buffer and injected to HiTrapTM Heparin HP column (GE Healthcare) pre-equilibrated with Buffer A (50 mM HEPES pH 7.5, 100 mM NaCl, 5% glycerol, 1 mM EDTA, 1 mM DTT), then the column was washed at 1 ml/min flow rate with a gradient 100–1000 mM NaCl. The eluted fractions
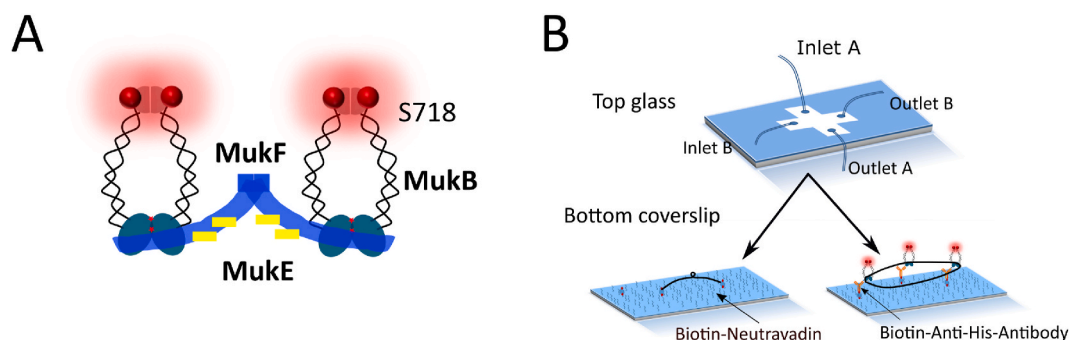

Fig.1. Single-molecule assays to study *E. coli* SMC complex, MukBEF. (A) Cartoon representation of MukBEF subunits and domains in different colors. MukF (blue) is kleisin protein which binds and bridges the ATPase head domains of the MukB dimers, and MukE (yellow) is KITE protein in *E. coli*. S718 at hinge domain [28] was mutated to unnatural amino acid (p-azido-ʟ-phenylalanine, AZF) and labelled with Cy5 (marked as red balls) via click chemistry. (B) Sketch of single molecule study. Top slide is designed for injection along two perpendicular directions. The bottom slide is to immobilize either MukB or DNA on the surface. In assay 1, 48.5 kbp λDNA was doubly tethered to the PEG modified surface. In assay 2, MukB was immobilized by using a His$_6$-tagged variant of MukB and biotinylated anti--His$_6$-antibody on the PEG surface.

were collected and dialyzed with dialysis buffer (25 mM HEPES pH 7.5, 25 mM KCl, 0.1 mM EDTA, 2 mM DTT, 1 mM PMSF, 5% Glycerol).

For the purification of His$_6$-tagged MukE and MuF, fractions from TALON resin were diluted and injected into HiTrap DEAE FF column (GE healthcare) pre-equilibrated in Buffer A, and then the column was washed at 1 ml/min flow rate with a gradient 100–1000 mM NaCl. The eluted fractions were collected and dialyzed with dialysis buffer. Protein concentration was estimated by UV absorption at 280 nm on Nanodrop and purity was confirmed by SDS-PAGE. Purified proteins were aliquoted, snap-frozen and stored at −80 °C until use.

2.7. Expression, purification and fluorescent labeling of the MukB His$_6$-tagged protein

To label MukB site-specifically, the unnatural amino acid *p*-azido-L-phenylalanine (AZP) was incorporated into the MukB [29]. The plasmid pBAD-MukB-S718TAG-10 GS-6×His was constructed as following: First, MukB gene was inserted into pBAD vector. MukB was 6×His-tagged at the C-terminus, and a flexible 10(glycine-serine) linker was introduced between His tag and MukB. Then an amber (TAG) codon was introduced at 718 position of the hinge domain of MukB by site-directed mutagenesis. To express MukB incorporated with AZP, pBAD-MukB--S718TAG-10 GS-6 × His plasmid and a pEvol plasmid containing the engineered Amber suppressor tRNA/synthetase system carrying a chloramphenicol resistance marker, were transformed into a derived strain (FW01) from C321ΔA strain, with chromosomal MukB tagged with 3XFlag.

2L cultures were grown in LB with 100 μg/ml carbenicillin, 25 μg/ml chloramphenicol and 1% glucose at 30 °C to OD600–0.6 with 1 mM *p*-azido-L-phenylalanine, and then induced by adding of L-arabinose at final concentration of 0.4% (W/V). After 4 h at 30 °C, cells were harvested by centrifugation, suspended in 30 ml lysis buffer (50 mM HEPES pH 7.5, 300 mM NaCl, 5% glycerol, 10 mM imidazole) supplemented with 1 tablet Complete mini-protease inhibitor cocktail (Roche) and sonicated. Cell debris was removed by centrifugation and target proteins were first purified by TALON Superflow resin. Then, the fractions from TALON were diluted to 100 mM NaCl buffer and injected to HiTrapTM Heparin HP column (GE Healthcare) pre-equilibrated with Buffer A (50 mM HEPES pH 7.5, 100 mM NaCl, 5% glycerol, 1 mM EDTA, 1 mM DTT), then the column was washed at 1 ml/min flow rate with a gradient 100–1000 mM NaCl. The eluted fractions were collected and the chromosomal MukB was removed by adding ANTI-FLAG M2 Affinity gel (A2220, Sigma) into the eluted fractions. After incubation for 30 min at 4 °C, and the gel was discarded by centrifugation. The supernatant was collected and concentrated by ultrafiltration.

The purified protein was labelled via copper free click chemistry. The protein was incubated with ~20 × molar excess of Dibenzylcyclooctyne (DBCO)-Sulfo-Cy5 (Jena Bioscience) at 4°C overnight in the dark. The Cy5 labelled MukB was purified by size-exclusion chromatography on a Superdex 200 10/300 GL column (GE Healthcare). Peak fractions were pooled and concentrated by ultrafiltration.

Labeling efficiency was estimated to be 65% based on the absorbance ratio of 280 and 650 nm, using the calculated molar extinction coefficient of MukB at 280 nm (335,670 M^{-1} cm^{-1}), the molar extinction coefficient of the Cy5 dye at 650 nm (250,000 cm-1M-1.), and correct factor for the absorption at 280 nm by the dye (ε^{280} nm/ε^{650} nm = 0.05).

2.8. Expression and purification of the MukE-Flag and MukF-Flag proteins

MukF Flag-tagged fragments were expressed from pET-21(+) plasmids in C3013I cells (NEB). The Flag-tagged MukE and MuF were at the C-terminus. pET-21(+)-MukE-C100S-Cys-Flag and pET-21(+)-MukF-C204S-Cys-Flag were constructed with the indigenous cysteines were removed and one cysteine was introduced at the C-terminus.

2L cultures were grown in LB at 37 °C to OD600~0.6 and induced by adding IPTG at final concentration of 1 mM. After 4 h at 30 °C, cells were harvested by centrifugation, suspended in lysis and binding buffer (50 mM HEPES pH 7.5, 150 mM NaCl, 10% glycerol, 1 mM EDTA) supplemented with 1 tablet Complete mini-protease inhibitor cocktail (Roche) and sonicated. Cell debris was removed by centrifugation and target proteins were incubated with 2 ml ANTI-FLAG M2 Affinity gel (A2220, Sigma) at 4°C for 4 h. The Flag tagged proteins were eluted out with high salt buffer (50 mM HEPES pH 7.5, 500 mM NaCl, 10% glycerol, 1 mM EDTA). The eluted fractions were collected and dialyzed with dialysis buffer. Purified protein was snap-frozen and stored at −80°C until use.

2.9. ATP Hydrolysis assays

ATP hydrolysis was analysed in steady state reactions using an ENZCheck Phosphate Assay Kit (Life Technologies). 150 μL samples containing standard reaction buffer supplemented with 2 mM of ATP were assayed in 18 BMG Labtech PherAstar FS plate reader at room temperature. The results were computed using MARS data analysis software. Quantitation of phosphate release was determined using the extinction coefficient of 11,200 M^{-1}cm^{-1} for the phosphate-dependent reaction at 360 nm at pH 7.0.

2.10. Mutagenesis

Point mutations in all constructs were made by using Q5 site-directed mutagenesis kit (NEB). Primers were designed with NEBase Changer. 10 ng of the template was taken to the reaction. Plasmids were isolated and mutations confirmed by sequencing.

2.11. Complementation assay

The assay relied on the ability of MukB expressed from pET-21(+) in the absence of IPTG (leaky expression) to complement growth defect of ΔmukB (RRL149) cells at non-permissive temperature (37°C). Cells were transformed with pET-21(+) carrying mukB or mukB variant and allowed to recover overnight post transformation at permissive temperature (22°C) on LB plates containing Carbenicillin (100 μg/ml) along with positive (pET-21(+) carrying WT-MukB) and negative (empty pET-21(+) vector) controls. Then single colonies were streaked onto two fresh plates and incubated at the permissive or non-permissive temperature to assay their ability to complement the growth deficiency.

3. Results

3.1. DNA compaction by MukB at low salt in the absence of ATP

Condensin and cohesin can compact DNA in the presence of ATP [10–12,30]. However, in assay 1 (Fig. 1B), no DNA compaction can be observed on the doubly tethered λDNA while incubation with 10 nM MukB, 20 nM MukE, 10 nM MukF and 1 mM ATP-Mg^{2+}(video S1). Fluorescently labelled MukB (MukB-Cy5) shows there is no MukBEF stable association with DNA during the observation time (Video S2). Importantly, fluorescent labelling does not affect MukBEF ATP hydrolysis activity (Fig.S2).

To examine the function of MukBEF carefully, we tested the MukBEF components sequentially. First, we incubated 10 nM MukB alone with DNA in the absence of flow, all slack λDNA molecules became tight **(compaction)** (Fig. 2A, video S3), and DNA 'bulbs' **(locally compacted DNA)** can be observed frequently (98.7%, 149/151 of DNAs, and Fig. 2F). DNA compaction is gradual over time (Fig. 2A and 2B) and the compaction rate is MukB concentration dependent, with higher compaction rate at higher concentration of MukB. For example, 10 nM MukB takes ~1000 s to fully compact DNA, while 100 nM MukB takes ~150 s (video S3 & video S4). We noticed that there is a 'threshold' protein concentration and salt sensitivity required for DNA compaction. For example, at 50 mM NaCl, 1 nM MukB alone cannot compact DNA,
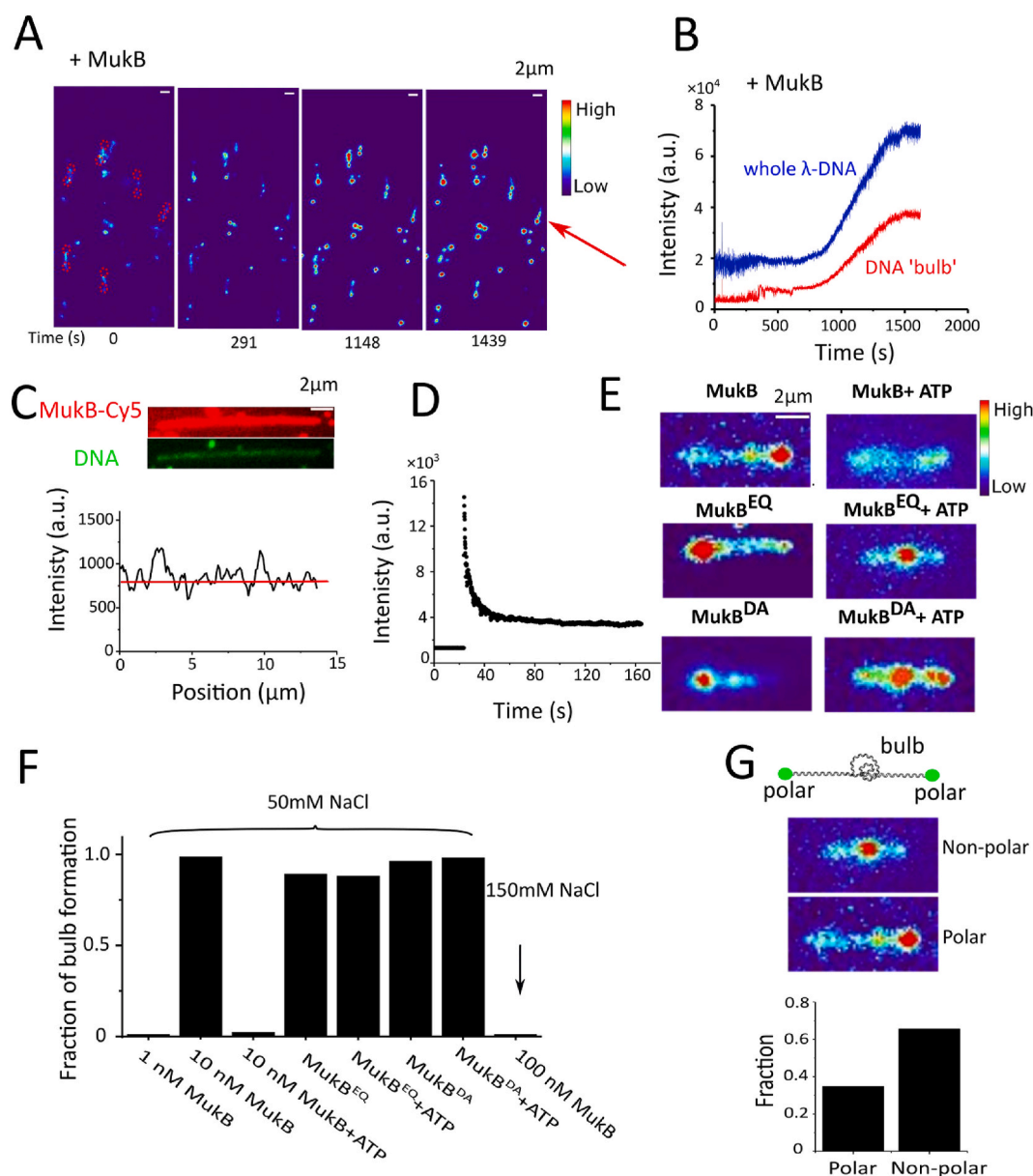
Fig.2. DNA compaction by MukB in the absence of ATP. (A) Time course showing DNA compaction by 10 nM MukB at 50 mM NaCl. DNA 'bulbs' are visible as bright dots on the doubly tethered λDNA. Two tethered ends are marked by red dashed circles. The red arrow shows one example of a doubly tethered λDNA. (B) The fluorescence intensity growing over time for whole λDNA (blue curve) and for DNA 'bulb' (red curve) as indicated by red arrow in Fig. 2A. The distance between two tethered ends is ~4 μm. We noticed that it was hard to quantify the compaction rate, as in TIRF microscope, the laser intensity decays exponentially with increasing distance from the interface; therefore, the intensity of entire λDNA is low at the beginning as most λDNA fragments are floating out of TIRF field. As time goes, more DNA is compacted coming close to the surface, and the increased intensity of 'DNA bulb' comes from two fractions: one from compacted DNA, and the other from the increased laser intensity close to the surface. (C) Distribution of Cy5 labelled MukB on over-stretched DNA (DNA curtain; video S5). The top panel shows two spectral channels: the red one is a snapshot of Cy5 labelled MukB, and the green one is a snapshot of Sytox orange stained DNA. The bottom panel is the fluorescence distribution of Cy5 along the DNA. (D) Bleaching curve of Cy5 in Fig. 2C over time, which indicates that many MukB molecules binding to DNA. (E) Snapshot examples of λDNA under different conditions. DNA compaction and DNA 'bulb' formation is induced by MukB only without ATP. However, 'bulbs' can be seen after addition of MukB^{EQ} and MukB^{DA}, both in the absence and presence of ATP. Scale bar 2 μm. (F) Fraction of DNA bulbs that formed on doubly tethered λDNA following incubation with the indicated components at different salt conditions. 50–150 DNAs were analysed. (G) Fraction of DNA 'bulbs' location. 240 DNAs were analysed. DNA 'bulbs' are located only by 34.6% (83/240 DNA bulbs) at the polar regions of tethered λDNA which indicates that 'DNA bulb' formation is not due to protein interaction between MukB and biotin/neutravidin on the surface.

and 'bulbs' are rarely observed even after 4 h (1.7%, 1/60 DNAs), while for concentrations larger than 10 nM, MukB can easily compact DNA and 'bulbs' are frequently observed (98.7%, 149/151 of DNAs). At 150 mM NaCl, even 100 nM MukB cannot compact DNA and 'bulbs' are rarely observed (0%, 0/58 DNAs, Fig. 2F). This compaction is not stable and can be easily destroyed by resuming high flow rates (>0.5 pN), and that DNA 'bulbs' cannot be expanded into loops at ~1 pN of applied

force.

Supplementary data related to this article can be found online at http s://doi.org/10.1016/j.bbrep.2022.101297.

To test whether MukB has a sequence preference for prominent loading sites to form 'bulbs', we over-stretched the DNA (similar as DNA curtain) and added 10 nM MukB-Cy5; a fairly homogenous distribution of MukB along the DNA can be observed (Fig. 2C & video S5), consistent

with MukB loading randomly onto DNA. The bleaching curve of MukB-Cy5 indicates multiple MukB molecules binding to DNA (Fig. 2D).

3.2. ATP inhibits MukB-mediated DNA compaction in the absence of MukEF

We further tested the function of ATP during DNA compaction by MukB. Strikingly, DNA cannot be compacted by MukB incubation with ATP-Mg^{2+} and no 'bulbs' can be seen on DNA (the fraction of DNA bulbs: 1.0%, (1/98 of DNAs) Fig. 2E & Fig. 2F). Meanwhile, the dwell time of MukB on DNA in the presence of ATP-Mg^{2+} was very short and stable association of MukB with DNA cannot be observed (video S6).

Constructs with EQ mutation in the SMC ATPase domain, where the two catalytic domains remain in an ATP engaged condition, are deficient in ATP hydrolysis and exhibit abnormally stable binding to DNA [31–33]. *In vivo* studies suggest that an EQ mutation holds together newly replicated chromosomes and inhibits chromosomes segregation [34], or inhibits the relocation of SMC proteins (MukBEF and cohesin) [35,36]. We further studied the EQ MukB mutant (MukB^{EQ}), which can bind but cannot hydrolyse ATP. Strikingly, MukB^{EQ} can fully compact DNA both in the presence and absence of ATP-Mg^{2+} at a MukB concentration above 10 nM (fraction of DNA bulbs: 90.2%, (46/51 of DNAs) and 88.0%, (103/117 of DNAs) Fig. 2E & Fig. 2F, video S7). Another DA mutation (MukB^{DA}) which cannot bind ATP, can also fully compact DNA both in the presence and absence of ATP-Mg^{2+} at a higher MukB concentration (100 nM) (fraction of DNA bulbs: 96.3%, (52/54 of DNAs) and 98.1%, (51/52 of DNAs) Fig. 2E & Fig. 2F). The EQ and DA mutation data suggest that ATP does not contribute directly to DNA compaction.

Supplementary data related to this article can be found online at http s://doi.org/10.1016/j.bbrep.2022.101297.

3.3. MukEF and ATP-Mg^{2+} conditionally stabilize pre-incubated MukB and DNA complex

MukEF depleted strains show the same temperature-sensitive growth phenotype as the MukB-null strain, and MukEF is essential for stable association of MukB with chromosome *in vivo* [37]. Thus, we further investigated the function of MukEF and ATP-Mg^{2+}, for which we first incubated 10 nM MukB with DNA at 50 mM NaCl until DNA is fully compacted, then flowed in MukEF with ATP-Mg^{2+}. We observed that DNA just becomes slack, and stable 'bulbs' can be observed (Fig. 3A& video S8) under high flow. Occasionally, these 'bulbs' can be expanded into 'loops', however, these loops do not grow in size over time. (Fig.3B & video S9). Most MukB was just washed off, with some clusters remaining on DNA, and quantification shows that the numbers of MukB varies. 84.1% (Fig. 3D) measured MukB shows the number between 2 and 4, which indicates that the major population of MukBEF clusters are dimers of homodimeric MukB. These 'bulbs' are very stable and remain associated with DNA even under ~2.5 pN of applied force.

Supplementary data related to this article can be found online at http s://doi.org/10.1016/j.bbrep.2022.101297.

Supplementary data related to this article can be found online at http s://doi.org/10.1016/j.bbrep.2022.101297.

3.4. Stable loop formation by MukB^{EQ}EF and ATP-Mg^{2+}

Because MukB^{EQ}EF can form clusters *in vivo* [35], we wanted to test the behaviour of MukB^{EQ}EF *in vitro*. Here, we observed that MukB^{EQ}EF forms clusters on the DNA with MukB^{EQ} EF and ATP-Mg^{2+}, and these MukB^{EQ}EF complexes are very stably associated on DNA with 150 mM NaCl buffer and at ~1 pN of applied force (Fig. 3E, Fig. S5A & video S10). DNA 'bulbs' can also be observed, and frequently these 'bulbs' can be expanded into 'loops' at ~1 pN of applied force, however, the loops don't grow in size over time even when applying ~1 pN force (Fig. 3E & video S11). Quantification shows that the number of MukB^{EQ}EF varies (Fig. 3J), and higher-number clusters appear more frequently compared

to the wt-MukBEF with ATP-Mg^{2+} (Fig. 3D and Fig. 3J). When we decreased MukB^{EQ} to 1 nM, stable association of MukB^{EQ} with DNA was also observed, however, without DNA 'bulbs' (Fig. 3F). We speculate that these DNA 'bulbs' and 'loops' are formed by dimerization of MukF, because they are very stable against high flow rates, in contrast to DNA 'bulbs' formed by MukB alone and which are not stable under high flow rates. To test this, we flowed in MukB^{EQ} with truncated MukF (Monomeric MukF, MonoMukF) which is monomeric in solution, being unable to form stable heads-engaged dimers [38]. Very stable protein complexes can be observed on DNA with MonoMukF with 150 mM NaCl buffer and at ~1 pN of applied force (Fig. S5B and video S12); however, DNA 'bulbs' or 'loops' were rarely observed. Quantification shows that 88.4% of cluster population contains less than 2 MukB^{EQ}, indicates MukB^{EQ} is a single dimer with MonoMukF (Fig. 3K).

Supplementary data related to this article can be found online at http s://doi.org/10.1016/j.bbrep.2022.101297.

3.5. DNA can be stretched on immobilized MukB and slides through MukB

To further investigate the dynamics of DNA under action of MukBEF, in assay 2, MukB was immobilized on the surface, and the interaction of DNA with MukB(EF) was analysed (Fig. 1B). First, we pre-incubated circular DNA (44 kb plasmid) with surface-immobilized MukB-His, as well as MukE-Flag, MukF-Flag and ATP-Mg^{2+} in solution; in this case, essentially no DNA spots were observed on the surface (Fig. 4A and video S13). However, upon incubation of MukB-His with plasmid DNA, many DNA spots can be observed on the surface (Fig. 4A & video S14). For the control, we barely observed any DNA spots on the biotinylated anti-His$_6$-antibody functionalized PEG surface in the absence of MukB-His, which indicates that the imaged DNA molecules are specifically captured by MukB. Under flow, we observed stretched plasmids on the surface and breaking of DNA, with laser excitation commonly triggering DNA sliding off the surface (Fig. 4B & video S15).

Supplementary data related to this article can be found online at http s://doi.org/10.1016/j.bbrep.2022.101297.

To test what happens to linear DNA, we first incubated MukB with λDNA at 50 mM NaCl, then flowed the mixture into the cell functionalized with biotinylated anti-His$_6$-antibody on the surface. Strikingly, λDNA can be easily stretched on the surface with many tether points and two DNA ends spinning round the tether points (Fig. 4C). At low concentration of MukB, λDNA was stretched only with two tether points, and laser-induced breaking of DNA commonly triggers DNA sliding off the tether points (Fig. 4C, D & video S16). Stretching DNA normally requires modification of DNA extremities to anchor DNA to a functionalized substrate, e.g., via sticky ends or biotin functionalization, and the bond strength between biotin and streptavidin is far beyond the weak electrostatic interaction between MukB and DNA (Fig. S3). Why could naked λDNA be stretched on the surface? One possibility is that the DNA is topologically entrapped in the MukB ring (Fig. 4E), which inhibits DNA detachment from the surface even under strong flow.

Supplementary data related to this article can be found online at http s://doi.org/10.1016/j.bbrep.2022.101297.

For open λDNA, it is very difficult to estimate the DNA length and thus to calculate the sliding speed, as many DNA fragments are floating out of the TIRF region. We managed to get two circular λDNA. After DNA breakage, λDNA slides on immobilized MukB and sequentially detaches (Fig. 4F & video S17). We further calculated the sliding speed for λDNA, which was ~2kbp/s (Fig. 4G). For plasmids, the sliding speed was ~5kbp/s, faster than for linear λDNA (Fig. 4G).

Supplementary data related to this article can be found online at http s://doi.org/10.1016/j.bbrep.2022.101297.

Supplementary data related to this article can be found online at http s://doi.org/10.1016/j.bbrep.2022.101297.
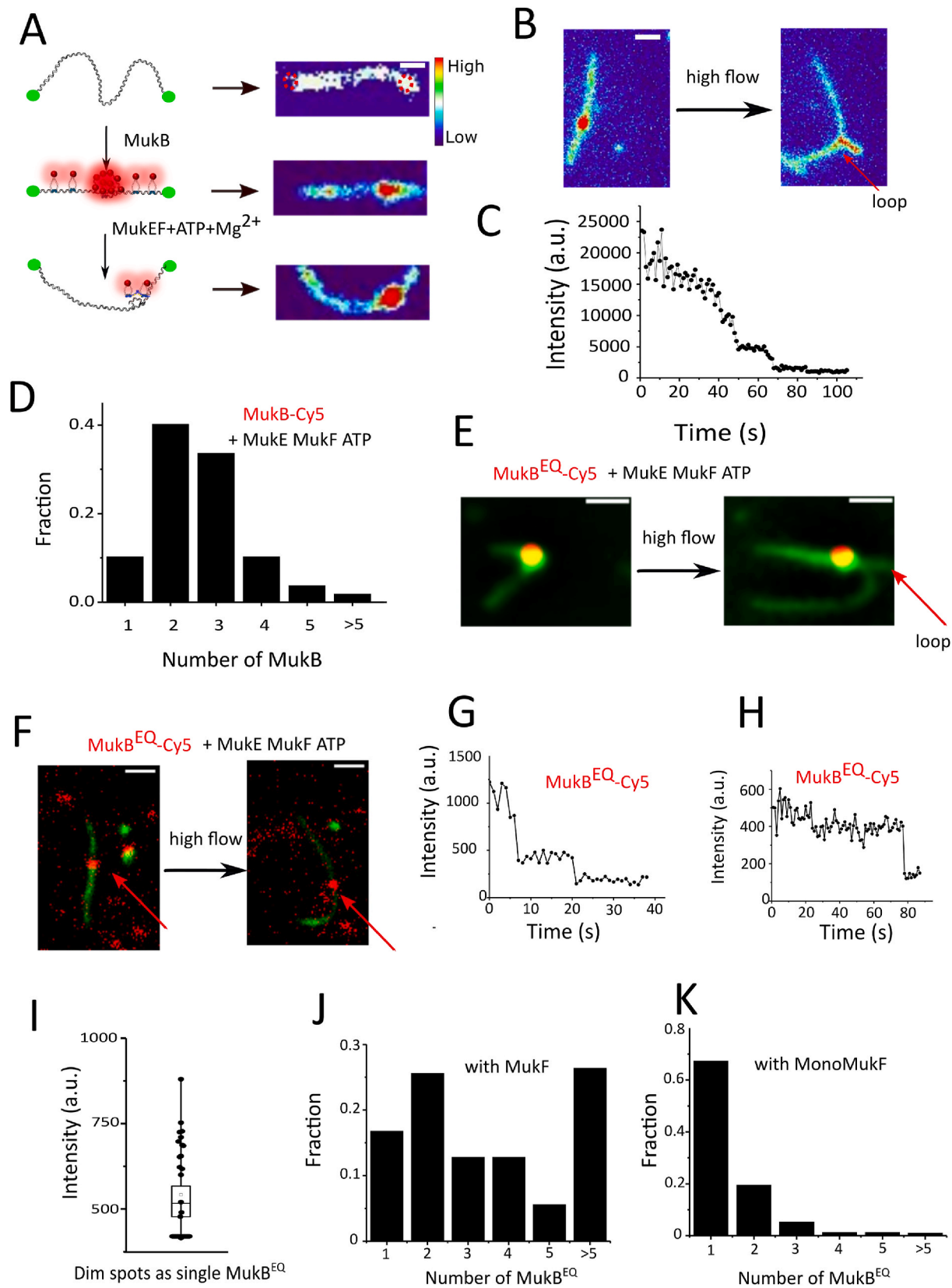
(caption on next page)

Fig.3. DNA compaction and loop formation under different conditions. (A) DNA 'bulbs' on the u-shaped double-tethered λDNA by MukBEF clusters with ATP-Mg^{2+}. First, λDNA was incubated with MukB until DNA is fully compacted, and afterwards, MukEF and ATP-Mg^{2+} were flowed into the chamber from a perpendicular direction. Scale bar 2 μm. The right panels show examplary snapshots of different DNA conformations. (B) One example of a 'bulb' formed in the presence of MukBEF clusters with ATP-Mg^{2+}. This 'bulb' can be expanded into loops at ~1 pN of applied force. The loop does not grow over time. Scale bar 2 μm. (C) Representative time traces of fluorescence intensities of MukBEF clusters with ATP-Mg^{2+}on tethered DNA. (D) The chart shows numbers of MukB clusters with ATP-Mg^{2+}on DNA 'bulbs' based on measuring the fluorescence intensity of the 'bulbs' and comparing it to that of a single MukB bound to glass (bleaching steps are too noisy for reliable quantification). Quantification shows 40.2% of 2-MukB, 33.6% of 3-MukB, and 10.3% of 4-MukB molecules; 107 DNAs were analysed. (E) Stable 'bulbs' and 'loops' can be easily observed when MukB^{EQ}, MukEF and ATP-Mg^{2+}are present. One example of a 'bulb' that can be expanded into a loop (red arrow) at ~1 pN of applied force (Video S11). Scale bar 2 μm. (F) Stable association of MukB^{EQ} can be easily observed on DNA at a decreased concentration of MukB^{EQ} (1 nM), MukE$_2$F (2 nM) in the presence of 1 mM ATP-Mg^{2+}. However, no 'bulbs' or 'loops' can be observed under flow. Labelled MukB^{EQ} (marked by red arrow) moves together with DNA, confirming that it was indeed stably bound to DNA. Scale bar 2 μm. (G) Representative two stepwise bleaching events of MukB^{EQ} in the presence of MukEF and ATP-Mg^{2+}. (H) Representative single step bleaching of MukB^{EQ} in the presence of MukEF and ATP-Mg^{2+}. (I) Intensity distribution of single MukB^{EQ} EF clusters on the surface. (J) The chart shows numbers of MukB^{EQ} on DNA 'bulbs' in the presence of MukEF and ATP-Mg^{2+}, based on measuring the fluorescence intensity of the 'bulbs' and comparing it to that of single MukB^{EQ} bound to glass. 125 clusters were analysed. (K) The chart shows numbers of MukB^{EQ} on DNA 'bulbs' in the presence of MukE, MonoMukF, and ATP-Mg^{2+}. 164 clusters were analysed.

3.6. MukE, MukF and ATP binding stabilizes MukB and DNA complex on the surface

To further investigate the function of MukEF and ATP-Mg^{2+}, we then flowed in MukE-Flag, MukF-Flag and ATP-Mg^{2+} in 150 mM NaCl buffer to investigate the behaviour of λDNA on tethered MukB; after these additions, most λDNA molecules were just washed off (Fig. 4H & video S18). When we flowed in MukE-Flag, MukF-Flag and ATP-Ca^{2+}, which is supposed to inhibit ATP hydrolysis of the nucleotide-binding domains [39], strikingly, most λDNA remained on the surface. We then significantly increased the flow rate up to 100ul/min (~2.5 pN) with MukE-Flag, MukF-Flag and ATP-Ca^{2+} in 150 mM NaCl, and all λDNA were over-stretched on the surface to linear conformations with a few tether points (Fig. 4I & video S19). We then increased the laser power to break DNA into pieces (Fig. 4I & video S19). Strikingly, λDNA does not slide off the surface, and the tether points remained on the surface. This suggests that without ATP hydrolysis, MukE, MukF and ATP stabilize the interaction between MukB and DNA, and this stabilized interaction can even resist high force (~2.5 pN).

4. Discussion and conclusions

Our results show that MukB alone can compact DNA under low salt conditions when MukB concentration is above a certain 'threshold' concentration. This is in agreement with previous studies that showed MukB alone can compact DNA [40–42]. As MukB dimers alone have negligible ATPase activity [43–45], the catalytic cycle of ATP hydrolysis may influence the dwell time of MukB on DNA by regulating MukB head opening/closing (Fig. 5A), when MukE and MukF are absent, and this could be the underlying reason why ATP inhibits MukB-mediated DNA compaction. This observation is in contrast to the previous *in vitro* study which suggests ATP induces DNA compaction by MukB [46].

There exists one core argument that MukBEF together with ATP-Mg^{2+} all are required for normal chromosome organization and segregation *in vivo*; while our *in vitro* single-molecule data shows that MukBEF together with ATP-Mg^{2+} seems to be incapable of remodelling DNA; only rare MukBEF clusters on DNA 'bulbs' were observed occasionally. Actually, this is in agreement with *in vivo* observations that even high concentrations of ~100 nM of (Muk4B:4E:2F) complexes at high density of DNA in *E.coli* (the density of DNA in *E.coli* is 10^5 times of DNA used in the single-molecule assay) result only in 48% loading on DNA with a dwell time of about ~60 s. The unloading rate (k_{off_MukBEF}) is ~0.015 s^{-1} (dwell time 65 s), and the loading rate *in vivo* (k_{on_MukBEF}) is only ~3.9*10^{-6} s^{-1} which would result in 48% occupancy of MukBEF on chromosome [35,47]. In the single-molecule assay, it requires $1/3.9*10^{-6} = 2.56*10^5$ s (~3 days) to capture a loading event in pre-incubated MukBEF solution, and that is also the reason why in an *in vitro* biochemistry assay which shows a 'fake' inhibition of MukEF to loading of MukB on DNA. The extremely low loading rate does also reveal that most collisions of MukBEF with DNA do not lead to loading,
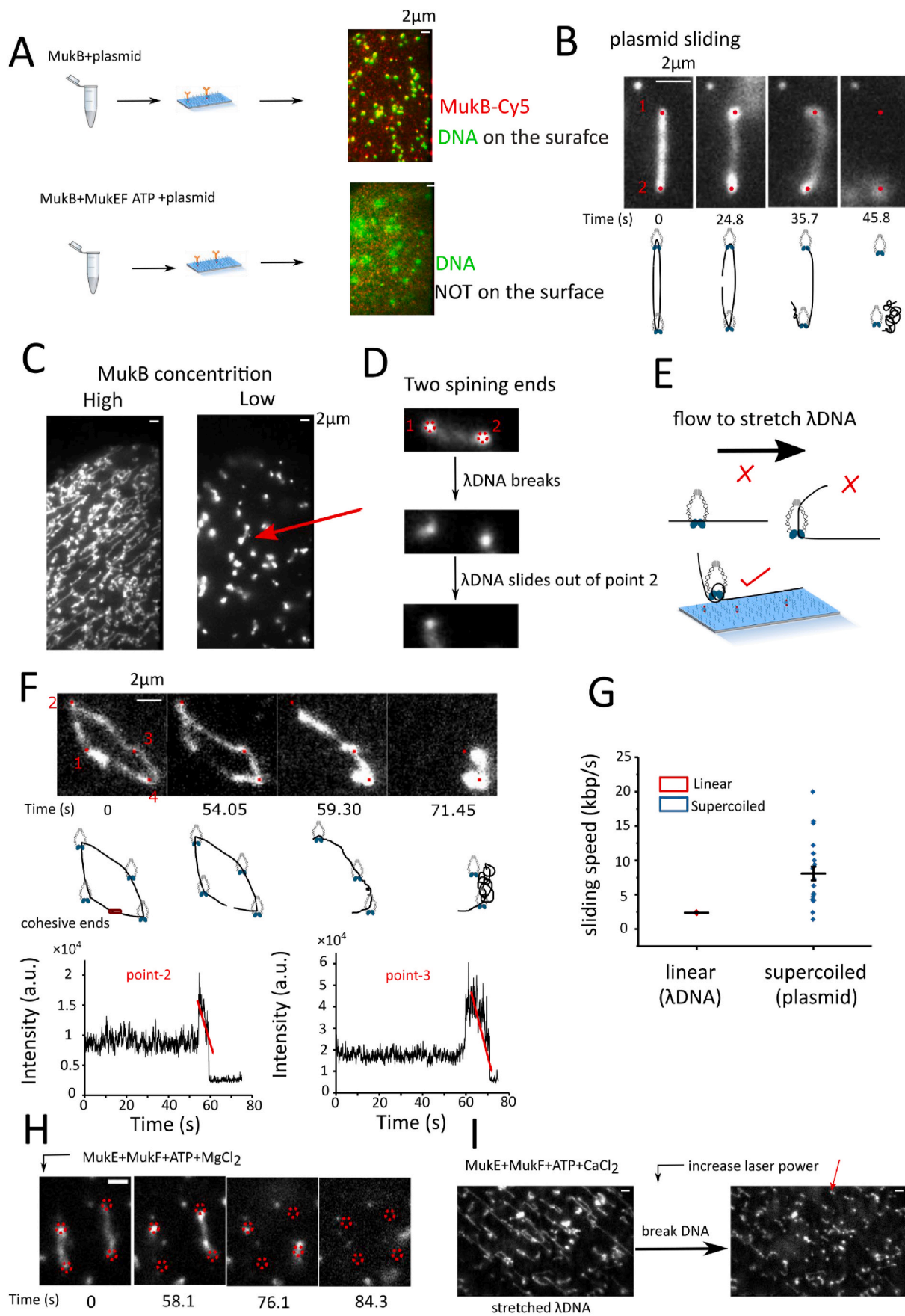
and there is a small chance that ATP binding or hydrolysis can trigger distinct conformational changes within the two head regions of MukBEF that could act synergistically to open the MukB ring for DNA loading/unloading. ATP hydrolysis is required to regulate MukB head opening/closing, and therefore regulates MukBEF loading/unloading on/from DNA to balance the numbers of MukBEF on DNA, as too many loops generated by MukBEF lead to over-compacted chromatin which may block chromosome replication, gene expression and regulation, whereas too few generated loops lead over-spread chromatin.

Pre-incubated MukBEF complexes rarely undergo stable association with DNA, while sequential incubation of MukB with DNA, and then MukEF and ATP-Mg^{2+}, can stabilize MukB/DNA interaction. Together with *in vivo* observations that MukEF is essential for stable association of MukB [37,48], these superficially conflicting observations may be reconciled by assuming that DNA binds MukB topologically (DNA wrapping around the head domains of MukB proposed model in Fig. 5B & video S20). Similar DNA wrapping mechanism has also been proposed by other studies [49–51]. Structural studies of wide-type SMC, instead of mutated SMC, would help to verify the DNA wrapping mechanism.

Supplementary data related to this article can be found online at https://doi.org/10.1016/j.bbrep.2022.101297.

Hydrolysis of ATP does only yield about 20 to 25 k_BT energy. Actually, it was shown that 80% of the input energy of ATP was dissipated into heat and did not contribute to power the motor protein kinesin [52]. The free energy released upon ATP hydrolysis is rapidly dissipated and it is the differential binding of ATP and its hydrolysis products ADP and Pi that leads to the slow conformational transitions of the motor protein [53]. Some studies also suggested that ATP hydrolysis is not involved in directional motion; rather, it drives SMC protein loading and unloading onto chromatin [54–56]. A relatively small force (entropic force) of k_BT/P is required to align elastic units of dsDNA, and this entropic force is ~0. 1 pN, within the range of external forces that were applied in this work, and also published for single-molecule experiments that observed DNA compaction or looping induced by cohesion and condensin [10,12,30,57]. Moreover, in cells, DNA can move or slide by itself if considering the elastic energy that DNA contains, such as supercoiling [58–61].

Our DNA-sliding ratchet model (Fig. 5C) does explain how MukBEF can efficiently organize DNA while having only low ATPase activity, and the intrinsic ability to entrap DNA topologically. This DNA sliding model can also explain the different behaviours of other SMC proteins. For example, cohesion complexes act differently in the presence of linear and circular DNA (not supercoiled) attached to beads under high salt concentration, where a cohesion complex can slide off the free ends of linear DNA, but gets trapped on circular DNA [62]. Nucleosomes containing ~150 base pairs of tightly wrapped DNA are the basic structural elements of chromatin compaction and regulation, while SMC proteins contribute to the large-scale chromosome organization and regulation. Nucleosomes do show sliding and loop formation [63–67]. Perhaps, SMC proteins and nucleosomes share a common DNA sliding, loop formation, and ratchet mechanism. Other SMC proteins can also be

Fig. 4. Immobilization of His$_6$-tagged MukB on the surface. (A) Upper panel: example of circular DNA (44 kb plasmid, green, Sytox orange staining) captured on the surface and incubated with His$_6$-tagged MukB. Lower panel: example of circular DNA diffusion in solution incubated with 10 nM MukB with 2 mM ATP+ 2 mM CaCl$_2$, +10 nM MukE +20 nM MukF (B) Sequential images of 44 kb plasmid sliding through MukB. Two red dots indicate the tether points. At ~24.8 s, the plasmid DNA breaks. At ~35.7 and ~45.8 s, the plasmid DNA slides through the tether points one after the other (Video S15). (C) Linear DNA (λDNA) can be stretched on surface with immobilized MukB. Left panel: 150 pM λDNA with 20 nM MukB, right panel: 150 pM λDNA with 5 nM MukB. Incubation buffer: 10 mM NaCl 20 mM Tris-HCl pH = 7.0. (D) One example with two DNA ends spinning round the tether points (Video S16). Red dashed circles indicate two captured points on the surface with immobilized MukB. DNA breaks and slides out of point-2. (E) λDNA topologically entrapped in the MukB ring can be stretched along the surface. (F) λDNA slides through immobilized MukB and is sequentially released. Sequential images of λDNA sliding across MukB. Series of snapshots showing Sytox orange-stained λDNA sliding through tethered MukBs one by one (Video S17). Four red dots indicate the tether points. At ~54 s, the cohesive end breaks. At ~59.3 s and ~71.45 s, the λDNA slides through the second and the third tether points, respectively. The DNA slides in a clockwise direction. Notably, the λDNA does not slide through the fourth tether point in anti-clockwise direction. Schematic diagrams under each snapshot are for visual guidance. Two plots monitor the DNA intensity around the tether points (point 2 and point 3) over time. The linear decay (red lines) indicates that the DNA release mechanism is by sliding, instead of multiple binding/unbinding. (G) Quantification of sliding speed of linear DNA (λDNA) and supercoiled DNA (44 kb plasmid). (H) Time course of captured λDNA on surface with immobilized MukB under high salt wash (150 mM) with MukE, MukF and ATP-Mg^{2+}. The capture points are marked by red dashed circles. One capture point was released from surface at 58.1 s, and two other points were released at 76.1 s, and the last capture point was released at 84.5 s (video S18). (I) Captured λDNA on surface with immobilized MukB under high salt wash (150 mM) with MukE, MukF and ATP-CaCl$_2$ (video S19). Left panel: λDNA is totally stretched on surface with the immobilized MukB. Right panel: laser excitation induces λDNA break, and DNA debris is still at the tether points on the surface. One examplary tether point is marked by red arrow.
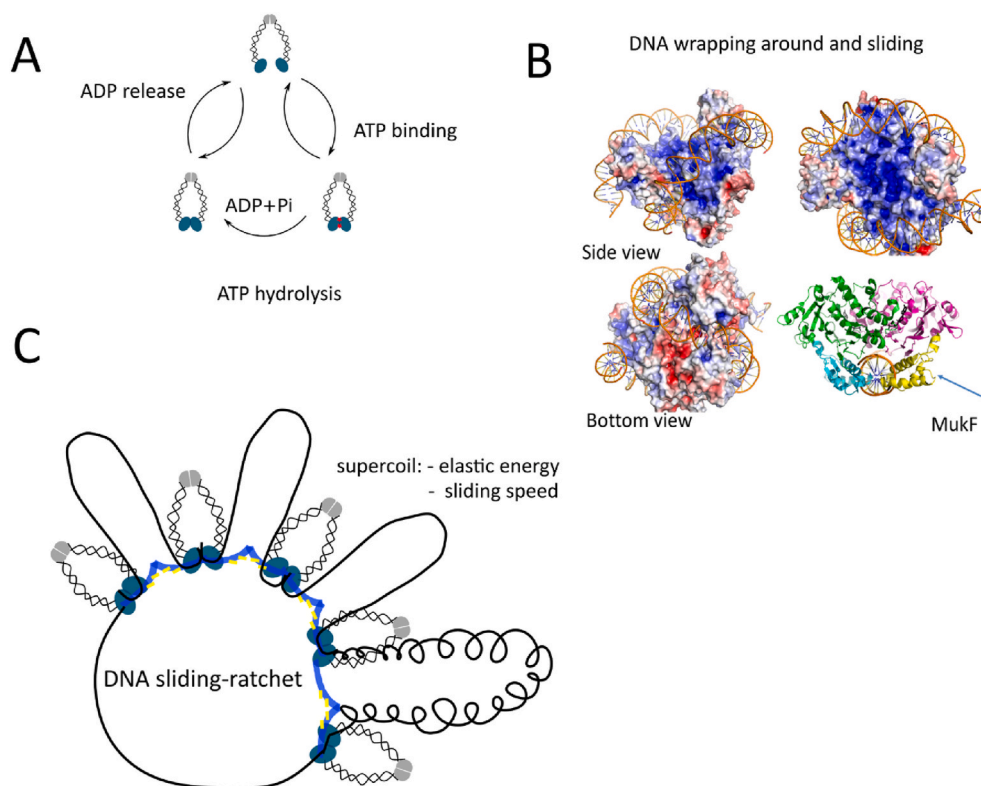

Fig.5. Kinetics of MukBEF loading/unloading on/from DNA and DNA-sliding ratchet model. (A) Kinetics of ATP hydrolysis cycle: ATP binding, ATP turn-over, and ADP releasing. The ATP hydrolysis regulates the MukB head opening/closing, and therefore regulates MukBEF loading/unloading on/from DNA. (B) DNA wrapping around the head domain of MukB (Proposed based on the published crystal structure [68]): DNA is topologically entrapped by a MukB head in the presence of the MukF C-terminus. C-terminus of MukF inserts into the groove of DNA (Video S20). (C) DNA-sliding ratchet model: the big loops are formed by dimerization of MukF. DNA slides through MukB to regulate loop size. Supercoiling of DNA, which is related to the elastic energy of DNA, may regulate the sliding speed.

immobilized on the surface to test this DNA sliding and ratchet mechanism. How SMC complexes facilitate DNA chromosome organization and segregation touches fundamental biological and physical questions: What are the molecular mechanisms of motor proteins? What is the contribution of entropy in the living cells? Although we cannot rule out complete answers for these questions, our results suggest a possible molecular mechanism of SMC protein, which could rationalize all the single-molecule observations in this study.

Author contributions

Man Zhou (M.Z.) and David Sherratt conceived and directed the project. M.Z. undertook biochemical experiments, single molecule experiments and undertook quantitative imaging and analysis. M. Z. wrote the manuscript.

Declaration of competing interest

The other authors declare that no competing interests exist.

Data availability

Data will be made available on request.

Leeds) helped with crystal structure modelling. We thank David Sherratt and, members of the Sherratt group and members of Kim Nasmyth group for helpful discussions. We thank Achillefs Kapanidis and Jörg Enderlein (Third Institute of Physics, University of Göttingen) for insightful discussion and constructive criticism of the manuscript. This work was supported by a Wellcome Investigator Award [200782/Z/16/Z to David Sherratt].

Appendix A. Supplementary data

Supplementary data to this article can be found online at https://doi.org/10.1016/j.bbrep.2022.101297.

References

[1] K. Nasmyth, C.H. Haering, The structure and function of SMC and kleisin complexes, Annu. Rev. Biochem. 74 (2005) 595–648.

[2] A.J. Wood, A.F. Severson, B.J. Meyer, Condensin and cohesin complexity: the expanding repertoire of functions, Nat. Rev. Genet. 11 (2010) 391–404.

[3] S. Gruber, MukBEF on the march: taking over chromosome organization in bacteria? Mol. Microbiol. 81 (2011) 855–859.

[4] S. Nolivos, D. Sherratt, The bacterial chromosome: architecture and action of bacterial SMC and SMC-like complexes, FEMS Microbiol. Rev. 38 (2014) 380–392.

[5] T. Terakawa, S. Bisht, J.M. Eeftens, C. Dekker, C.H. Haering, E.C. Greene, The condensin complex is a mechanochemical motor that translocates along DNA, Science 358 (2017) 672–676.

[6] M. Kanke, E. Tahara, P.J. Huis in't Veld, T. Nishiyama, Cohesin acetylation and Wapl-Pds5 oppositely regulate translocation of cohesin along DNA, EMBO J. 35 (2016) 2686–2698.

[7] H. Kim, J.J. Loparo, Multistep assembly of DNA condensation clusters by SMC, Nat. Commun. 7 (2016) 1–12.

[8] J. Stigler, G. Çamdere, D.E. Koshland, E.C. Greene, Single-molecule imaging reveals a collapsed conformational state for DNA-bound cohesin, Cell Rep. 15 (2016) 988–998.

[9] I.F. Davidson, D. Goetz, M.P. Zaczek, M.I. Molodtsov, P.J. Huis, Veld in 't, F. Weissmann, G. Litos, D.A. Cisneros, R. Ladurner, F. Uhlmann, A. Vaziri, J. Peters, Rapid movement and transcriptional re-localization of human cohesin on DNA, EMBO J. 35 (2016) 2671–2685.

[10] M. Ganji, I.A. Shaltiel, S. Bisht, E. Kim, A. Kalichava, C.H. Haering, C. Dekker, Real-time imaging of DNA loop extrusion by condensin, Science 360 (2018) 102–105.

[11] I.F. Davidson, B. Bauer, D. Goetz, W. Tang, G. Wutz, J.-M. Peters, DNA loop extrusion by human cohesin, Science 366 (2019) 1338–1345.

[12] Y. Kim, Z. Shi, H. Zhan, I.J. Finkelstein, H. Yu, Human cohesin compacts DNA by loop extrusion, Science 366 (2019) 1345–1349.

[13] E. Kim, J. Kerssemakers, I.A. Shaltiel, C.H. Haering, C. Dekker, DNA-loop extruding condensin complexes can traverse one another, Nature 579 (2020) 438–442.

[14] J. Pelletier, K. Halvorsen, B. Ha, R. Paparcone, S.J. Sandler, C.L. Woldringh, W. P. Wong, S. Jun, Physical manipulation of the Escherichia coli chromosome reveals its soft nature, Proc. Natl. Acad. Sci. USA 109 (2012) E2649–E2656.

[15] C. Jeon, Y. Jung, B. Ha, A ring-polymer model shows how macromolecular crowding controls chromosome-arm organization in Escherichia coli, Sci. Rep. 7 (2017) 1–10.

[16] D. Marenduzzo, C. Micheletti, P.R. Cook, Entropy-driven genome organization, Biophys. J. 90 (2006) 3712–3721.

[17] S. Jun, B. Mulder, Entropy-driven spatial organization of highly confined polymers : lessons for the bacterial chromosome, Proc. Natl. Acad. Sci. USA 103 (2006) 12388–12393.

[18] S. Jun, A. Wright, Entropy as the driver of chromosome segregation, Nat. Rev. Microbiol. 8 (2010) 600–607.

[19] M. Bohn, D.W. Heermann, Repulsive forces between looping chromosomes induce entropy-driven segregation, PLoS One 6 (2011), e14428.

[20] I.F. Lau, S.R. Filipe, B. Søballe, O.A. Økstad, F.X. Barre, D.J. Sherratt, Spatial and temporal organization of replicating Escherichia coli chromosomes, Mol. Microbiol. 49 (2003) 731–743.

[21] J.K. Fisher, A. Bourniquel, G. Witz, B. Weiner, M. Prentiss, N. Kleckner, Four-dimensional imaging of E. coli nucleoid organization and dynamics in living cells, Cell 153 (2013) 882–895.

[22] C.A. Brackley, J. Johnson, D. Michieletto, A.N. Morozov, M. Nicodemi, P.R. Cook, D. Marenduzzo, Nonequilibrium chromosome looping via molecular slip links, Phys. Rev. Lett. 119 (2017) 1–5.

[23] C.A. Miermans, C.P. Broedersz, Bacterial chromosome organization by collective dynamics of SMC condensins, J. R. Soc. Interface 15 (2018), 20180495.

[24] E.J. Banigan, A.A. van den Berg, H.B. Brandão, J.F. Marko, L.A. Mirny, Chromosome organization by one-sided and two-sided loop extrusion, Elife 9 (2020) 1–46.

[25] J.F. Marko, P. De Los Rios, A. Barducci, S. Gruber, DNA-segment-capture model for loop extrusion by structural maintenance of chromosome (SMC) protein complexes, Nucleic Acids Res. 47 (2019) 6956–6972.

[26] S.K. Nomidis, E. Carlon, S. Gruber, J.F. Marko, DNA tension-modulated translocation and loop extrusion by SMC complexes revealed by molecular dynamics simulations, bioRxiv (2021).

[27] Y. He, J. Lawrimore, D. Cook, E.E. Van Gorder, S.C. De Larimat, D. Adalsteinsson, M.G. Forest, K. Bloom, Statistical mechanics of chromosomes: in vivo and in silico approaches reveal high-level organization and structure arise exclusively through mechanical feedback between loop extruders and chromatin substrate properties, Nucleic Acids Res. 48 (2020) 11284–11303.

[28] T.E. Melby, C.N. Ciampaglio, G. Briscoe, H.P. Erickson, The symmetrical structure of structural maintenance of chromosomes (SMC) and MukB proteins: long, antiparallel coiled coils, folded at a flexible hinge, J. Cell Biol. 142 (1998) 1595–1604.

[29] J.W. Chin, S.W. Santoro, A.B. Martin, D.S. King, L. Wang, P.G. Schultz, Addition of p-azido-L-phenylalanine to the genetic code of Escherichia coli, J. Am. Chem. Soc. 124 (2002) 9026–9027.

[30] T.R. Strick, T. Kawaguchi, T. Hirano, Real-time detection of single-molecule DNA compaction by condensin I, Curr. Biol. 14 (2004) 874–880.

[31] J.E. Moody, L. Millen, D. Binns, J.F. Hunt, P.J. Thomas, Cooperative, ATP-dependent association of the nucleotide binding cassettes during the catalytic cycle of ATP-binding cassette transporters, J. Biol. Chem. 277 (2002) 21111–21114.

[32] M. Hirano, T. Hirano, Positive and negative regulation of SMC-DNA interactions by ATP and accessory proteins, EMBO J. 23 (2004) 2664–2673.

[33] R. Vazquez Nunez, L.B. Ruiz Avila, S. Gruber, Transient DNA occupancy of the SMC interarm space in prokaryotic condensin, Mol. Cell. 75 (2019) 209–223.

[34] M.A. Schwartz, L. Shapiro, An SMC ATPase mutant disrupts chromosome segregation in Caulobacter, Mol. Microbiol. 82 (2011) 1359–1374.

[35] A. Badrinarayanan, R. Reyes-Lamothe, S. Uphoff, M.C. Leake, D.J. Sherratt, In vivo architecture and action of bacterial structural maintenance of chromosome proteins, Science 338 (2012) 528–531.

[36] B. Hu, T. Itoh, A. Mishra, Y. Katoh, K.L. Chan, W. Upcher, C. Godlee, M.B. Roig, K. Shirahige, K. Nasmyth, ATP hydrolysis is required for relocating cohesin from sites occupied by its Scc2/4 loading complex, Curr. Biol. 21 (2011) 12–24.

[37] W. She, Q. Wang, E.A. Mordukhova, V.V. Rybenkov, MukEF is required for stable association of MukB with the chromosome, J. Bacteriol. 189 (2007) 7062–7068.

[38] K.V. Rajasekar, R. Baker, G.L.M. Fisher, J.R. Bolla, J. Mäkelä, M. Tang, K. Zawadzka, O. Koczy, F. Wagner, C.V. Robinson, L.K. Arciszewska, D.J. Sherratt, Dynamic architecture of the Escherichia coli structural maintenance of chromosomes (SMC) complex, MukBEF, Nucleic Acids Res. 47 (2019) 9696–9707.

[39] S. Morbach, S. Tebbe, E. Schneider, The ATP-binding cassette (ABC) transporter for maltose/maltodextrins of Salmonella typhimurium, J. Biol. Chem. 268 (1993) 18617–18621.

[40] S. Bahng, R. Hayama, K.J. Marians, MukB-mediated catenation of DNA is ATP and MukEF independent, J. Biol. Chem. 291 (2016) 23999–24008.

[41] Y. Cui, Z.M. Petrushenko, V.V. Rybenkov, MukB acts as a macromolecular clamp in DNA condensation, Nat. Struct. Mol. Biol. 15 (2008) 411–418.

[42] Z.M. Petrushenko, Y. Cui, W. She, V.V. Rybenkov, Mechanics of DNA bridging by bacterial condensin MukBEF in vitro and in singulo, EMBO J. 29 (2010) 1126–1135.

[43] Z.M. Petrushenko, C.H. Lai, R. Rai, V.V. Rybenkov, DNA reshaping by MukB: right-handed knotting, left-handed supercoiling, J. Biol. Chem. 281 (2006) 4606–4615.

[44] J.S. Woo, J.H. Lim, H.C. Shin, M.K. Suh, B. Ku, K.H. Lee, K. Joo, H. Robinson, J. Lee, S.Y. Park, N.C. Ha, B.H. Oh, Structural studies of a bacterial condensin complex reveal ATP-dependent disruption of intersubunit interactions, Cell 136 (2009) 85–96.

[45] K. Zawadzka, P. Zawadzki, R. Baker, K.V. Rajasekar, F. Wagner, D.J. Sherratt, L. K. Arciszewska, MukB ATPases are regulated independently by the N-and C-terminal domains of MukF kleisin, Elife 7 (2018), e31522.

[46] N. Chen, A.A. Zinchenko, Y. Yoshikawa, S. Araki, S. Adachi, M. Yamazoe, S. Hiraga, K. Yoshikawa, ATP-induced shrinkage of DNA with MukB protein and the MukBEF complex of escherichia coli, J. Bacteriol. 190 (2008) 3731–3737.

[47] J. Mäkelä, D.J. Sherratt, Organization of the Escherichia coli chromosome by a MukBEF axial core, Mol. Cell. 78 (2020) 250–260.

[48] K. Ohsumi, M. Yamazoe, S. Hiraga, Different localization of SeqA-bound nascent DNA clusters and MukF-MukE-MukB complex in Escherichia coli cells, Mol. Microbiol. 40 (2001) 835–845.

[49] Q. Wang, E.A. Mordukhova, A.L. Edwards, V.V. Rybenkov, Chromosome condensation in the absence of the non-SMC subunits of MukBEF, J. Bacteriol. 188 (2006) 4431–4441.

[50] D.P. Bazett-Jones, K. Kimura, T. Hirano, Efficient supercoiling of DNA by a single condensin complex as revealed by electron spectroscopic imaging, Mol. Cell. 9 (2002) 1183–1190.

[51] R.B. Case, Y.P. Chang, S.B. Smith, J. Gore, N.R. Cozzarelli, C. Bustamante, The bacterial condensin MukBEF compacts DNA into a repetitive, stable structure, Science 305 (2004) 222–227.

[52] T. Ariga, M. Tomishige, D. Mizuno, Nonequilibrium energetics of molecular motor kinesin, Phys. Rev. Lett. 121 (2018) 218101.

[53] W. Hwang, M. Karplus, Structural basis for power stroke vs. Brownian ratchet mechanisms of motor proteins, Proc. Natl. Acad. Sci. U.S.A. 116 (2019) 19777–19785.

[54] B. Hu, T. Itoh, A. Mishra, Y. Katoh, K.L. Chan, W. Upcher, C. Godlee, M.B. Roig, K. Shirahige, K. Nasmyth, ATP hydrolysis is required for relocating cohesin from sites occupied by its Scc2/4 loading complex, Curr. Biol. 21 (2011) 12–24.

[55] Y. Murayama, F. Uhlmann, DNA entry into and exit out of the cohesin ring by an interlocking gate mechanism, Cell 163 (2015) 1628–1640.

[56] L. Wilhelm, F. Bürmann, A. Minnen, H.C. Shin, C.P. Toseland, B.H. Oh, S. Gruber, SMC condensin entraps chromosomal DNA by an ATP hydrolysis dependent loading mechanism in Bacillus subtilis, Elife 4 (2015) 1–18.

[57] M. Sun, T. Nishino, J.F. Marko, The SMC1-SMC3 cohesin heterodimer structures DNA through supercoiling-dependent loop formation, Nucleic Acids Res. 41 (2013) 6149–6160.

[58] R.E. Depew, J.C. Wang, Conformational fluctuations of DNA helix, Proc. Natl. Acad. Sci. USA 72 (1975) 4275–4279.

[59] A.V. Vologodskii, A.V. Lukashin, V.V. Anshelevich, M.D. Frank-Kamenetskii, Fluctuations in superhelical DNA, Nucleic Acids Res. 6 (1979) 967–982.

[60] J.F. Marko, E.D. Siggia, Fluctuations and supercoiling of DNA, Science 265 (1994) 506–508.

[61] J. Langowski, W.K. Olson, S.C. Pedersen, I. Tobias, T.P. Westcott, Y. Yang, DNA supercoiling, localized bending and thermal fluctuations, Trends Biochem. Sci. 21 (1996) 50.

[62] T.L. Higashi, P. Eickhoff, J.S. Sousa, J. Locke, A. Nans, H.R. Flynn, A.P. Snijders, G. Papageorgiou, N. O'Reilly, Z.A. Chen, F.J. O'Reilly, J. Rappsilber, A. Costa, F. Uhlmann, A structure-based mechanism for DNA entry into the cohesin ring, Mol. Cell. 79 (2020) 917–933.

[63] A. Saha, J. Wittmeyer, B.R. Cairns, Chromatin remodeling by RSC involves ATP-dependent DNA translocation, Genes Dev. 16 (2002) 2120–2134.

[64] I. Whitehouse, C. Stockdale, A. Flaus, M.D. Szczelkun, T. Owen-Hughes, Evidence for DNA translocation by the ISWI chromatin-remodeling enzyme, Mol. Cell Biol. 23 (2003) 1935–1945.

[65] K.K. Sinha, J.D. Gross, G.J. Narlikar, Distortion of histone octamer core promotes nucleosome mobilization by a chromatin remodeler, Science 355 (2017) eaaa3761.

[66] Y. Zhang, C.L. Smith, A. Saha, S.W. Grill, S. Mihardja, S.B. Smith, B.R. Cairns, C. L. Peterson, C. Bustamante, DNA translocation and loop formation mechanism of chromatin remodeling by SWI/SNF and, RSC. *Mol. Cell.* 24 (2006) 559–568.

[67] G. Lia, E. Praly, H. Ferreira, C. Stockdale, Y.C. Tse-Dinh, D. Dunlap, V. Croquette, D. Bensimon, T. Owen-Hughes, Direct observation of DNA distortion by the RSC complex, Mol. Cell. 21 (2006) 417–425.

[68] J.S. Woo, J.H. Lim, H.C. Shin, M.K. Suh, B. Ku, K.H. Lee, K. Joo, H. Robinson, J. Lee, S.Y. Park, N.C. Ha, B.H. Oh, H. Robinson, J. Lee, S.Y. Park, N.C. Ha, B.H. Oh, H. Robinson, J. Lee, S.Y. Park, N.C. Ha, B.H. Oh, Structural studies of a bacterial condensin complex reveal ATP-dependent disruption of intersubunit interactions, Cell 136 (2009) 85–96.